Chemical Physics Letters 516 (2011) 1–11

Contents lists available at ScienceDirect

Chemical Physics Letters

journal homepage: www.elsevier.com/locate/cplett

FRONTIERS ARTICLE

Fluorescence correlation spectroscopy as a tool for measuring the rotational diffusion of macromolecules

Christoph M. Pieper, Jörg Enderlein *

III. Institute of Physics – Biophysics, Georg August University, Friedrich-Hund-Platz 1, 37077 Göttingen, Germany

ARTICLE INFO

Article history:
Available online 7 July 2011

ABSTRACT

We give an overview of using fluorescence correlation spectroscopy (FCS) for measuring rotational diffusion of macromolecules, and present a new experimental scheme, pulsed-interleaved excitation or PIE-FCS, which allows for measuring all conceivable correlation curves of a polarization-sensitive FCS experiment. After giving a brief review of the theoretical foundations, we systematically study the impact of different experimentally relevant parameters such as depolarization by the objective, or non-collinearity between absorption and emission dipole of the fluorescent label. We also discuss the possibility to extract information about anisotropic rotational diffusion, and exemplify that by determining the size and shape of the large protein aldolase.

1. Introduction

Molecules and small particles suspended in solution undergo constant translational and rotational diffusion due to thermal motion. Measurement of the translational and rotational diffusion constants can give information about their size and shape. The most powerful methods for determining structural information on molecules in solution are NMR relaxation spectroscopy [1], and small angle X-ray scattering (SAXS) [2]. However, both methods are technically challenging, expensive, and require rather large amounts of sample, which all restrict their use as an everyday routine tool. Dynamic light scattering [3] is much less technically demanding, and yields size and overall shape information of macromolecules. But it, too, requires large sample concentrations, and their accuracy goes down with decreasing molecular size. Luminescence-based methods are much less demanding in regard to sample concentration, due to the enormous sensitivity and excellent signal-to-noise ratio achievable in luminescence detection. The classical luminescence-based method for rotational diffusion measurements is fluorescence anisotropy decay spectroscopy [4]. However, this method is only applicable if the fluorescence decay time of the employed fluorescent/luminescent label is of the same order of magnitude as the rotational diffusion time one wants to observe. However, the vast majority of fluorescent labels has fluorescence decay times on the order of a few nanoseconds, whereas rotational diffusion times of biological macromolecules such as globular proteins in aqueous solution at physiological temperatures exhibit rotational diffusion times of dozens to hundreds of nanoseconds. One potential way out of this problem is to use exotic luminescent labels with exceptionally long decay times such as rare-earth complexes or phosphorescent probes that emit light upon return form the triplet to the ground state, see e.g. [5–7]. However, there are several limitations preventing a broad application of these probes: (i) the emission intensity is often rather weak when compared with good fluorescent dyes, (ii) the intrinsic polarization anisotropy of the labels can be very low (due to non-dipolar electronic transitions), preventing their applicability as fluorescence anisotropy probes, (iii) it is difficult to label a given macromolecule in such a way that the probe co-rotates with the macromolecule.

An attractive but lesser known alternative to the above mentioned methods is fluorescence correlation spectroscopy (FCS). In FCS, one measures the correlation of the fluctuating fluorescence signal coming from a sample of fluorescent or fluorescently labeled molecules (or particles) at very low concentration (typically pico- to nanomolar). FCS was introduced in the early seventies by Magde et al. [8–10], and has since then seen a tremendous development. One of its major applications is the measurement of the translational diffusion of molecules in solution, which gives information about the molecular size of the studied molecular species. In recent years, fluorescence cross-correlation techniques have also gained enormous popularity for the measurement of binding and interaction between different molecular species. Excellent reviews can be found in Ref. [11]. That FCS can also be used for measuring rotational diffusion is less known, although this option was already clear at the very beginning of FCS [12–14]. The first successful

* Corresponding author.
E-mail addresses: pieper@physik3.gwdg.de (C.M. Pieper), enderlein@physik3.gwdg.de (J. Enderlein).

0009-2614/$ - see front matter © 2011 Elsevier B.V. All rights reserved.
doi:10.1016/j.cplett.2011.06.091

FCS measurements of rotational diffusion appeared only in the eighties [15,16], and recent advances in detector technology, optics, and high-speed electronics have made such measurements readily available [17–19]. However, up to this day, FCS did not find broad application for rotational diffusion measurements. There are several reasons for that. First, using FCS for rotational diffusion measurements is experimentally more demanding than using it for standard translational diffusion or cross-correlation measurements. To begin with, one needs polarized excitation and polarization-sensitive detection. Moreover, due to the fact that rotational diffusion of typical macromolecules takes places on times scales of dozens to hundreds of nanoseconds, one needs a detection scheme that allows for recording light with nanosecond temporal resolution and for cross-correlating photons on that time scale. Due to the finite dead-time of photodetectors (typically single-photon avalanche diodes), this requires the usage of at least two detectors in a Hanbury-Twiss-Brown scheme, see e.g. [17]. If one wants to record FCS curves for all possible combinations of excitation and detection polarization, one needs even a four-detector scheme, see below. Second, the theory of FCS with rotational diffusion is demanding (see Section 2). Third, there is no systematic study of how rotational diffusion measurements are influenced by such effects as depolarization when focusing/detecting light through objectives with large numerical aperture [20], label stoichiometry, non-zero angle between excitation/emission dipole of the label, overlap between the time scale of fluorescence decay and rotational diffusion, or insufficient co-rotation of the label with the labeled molecule. All these effects have to be taken into account of a complete and correct analysis of the FCS data. Last but not least, for a broad applicability of FCS for rotational diffusion measurements, one needs fluorescence labels having optimal fluorescence properties (convenient excitation/emission wavelength, high photo-stability and quantum yield), that can be rigidly attached to the macromolecules of interest such as proteins, and that are widely available and affordable.

In the present mini-review, we describe how to use FCS for rotational diffusion measurement, explaining all the necessary theoretical background, and the details of the experimental setup, measurement, and labeling. Moreover, we discuss in detail the impact of all the aforementioned potential complications such as light depolarization, label stoichiometry, or non-collinearity of excitation and emission dipole. We also present a recently developed measurement scheme [19] allowing for the measurement of *all* physically possible correlation curves, and we show that this ability becomes important when aiming at using FCS for extracting information about *molecular shape* and not only size. We hope that this review will help to make FCS a more attractive method for rotational diffusion measurements of macromolecules or colloids, exploiting its ability to measure at minute concentrations with highest sensitivity.

2. Theory

There are numerous theoretical studies available that are concerned with correlation measurements of rotational diffusion. These relate not only to FCS [13], but also to light scattering [3] and NMR. Nonetheless, we will briefly recapitulate the theoretical basis here to make the Letter self-consistent, trying to present the material in a form as lucid and transparent as possible, and to make it more easily understandable for the audience without a deep background in theoretical physics. Moreover, we will emphasize aspects and make approximations that are especially important for modern FCS measurements, and present the theory in such a general form as to include our newly developed measurement scheme that uses pulsed interleaved excitation for extracting all physically possible correlation curves (see also Section 4).

2.1. Correlation function

The experimental system which we will consider here is schematically shown in Figure 1. The sample is excited by linearly polarized lasers, where in the general setup one can switch between two orthogonal excitation polarizations. Detection is done in a polarization-sensitive manner with four detectors, as shown in the figure, so that one can obtain the second-order correlation function for any combination of excitation and detection polarizations.

These correlation functions are defined as

$$g_{ab}^{\alpha\beta}(t) = \langle I_a^{\alpha}(t_0) I_b^{\beta}(t_0 + t) \rangle_{t_0} \tag{1}$$

where $I_a^{\alpha}(t)$ is the signal detected by detector α at time after excitation with laser a, and the angular brackets with subscript t_0 denote time averaging over time t_0. On a pico- to nanosecond timescale, the correlation function is characterized by fluorescence antibunching and rotational diffusion. Fluorescence antibunching is caused by the fact that a single emitter with a finite lifetime of its excited state can emit only one photon at a time. It can be used to obtain the average number of emitters within the detection volume. Rotational diffusion will be seen in the correlation functions because a molecule can rotate between two subsequent photon excitation/emission events and thus rotate the molecule's dipole axis into or out of the polarization plane of a detector.

Let us consider an experiment using the setup shown in Figure 1. The sample should be excited by two consecutive laser pulses with negligible pulse width and with a temporal delay p between the two pulses. Let us now ask: what is the chance to detect two photons from one and the same molecule with lag time t between them? For the sake of simplicity let us assume that the fluorescence decay is mono-exponential with decay time τ, so that the chance to observe a photon a time t after an exciting laser pulse is given by the probability density $\exp(-t/\tau)/\tau$. If we take further into account that a molecule can emit, after one excitation pulse,

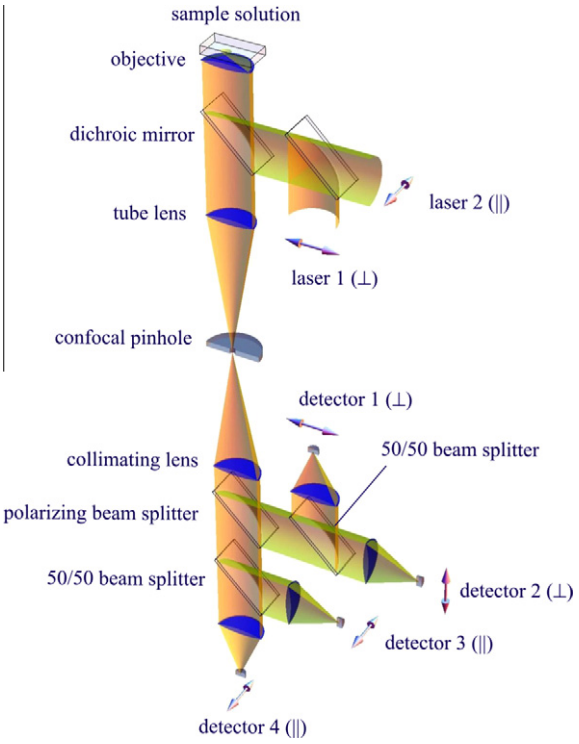

Figure 1. Schematic of the measurement set-up showing the polarization directions in the excitation and detection paths.

only one photon, the probability density for observing two photons with lag time t in between will be proportional to

$$\int_{\max(p-t,0)}^{p} dt' \frac{\kappa_a^\alpha}{\tau} e^{-t'/\tau} \frac{\kappa_b^\beta}{\tau} e^{-(t'+t-p)/\tau} = \kappa_a^\alpha \kappa_b^\beta F_1(t,\tau,p) \tag{2}$$

where we have introduced the abbreviation

$$F_1(t,\tau,p) = \frac{1}{\tau} \begin{cases} \sinh(t/\tau) e^{-p/\tau}, & t \leqslant p \\ \sinh(p/\tau) e^{-t/\tau}, & t > p \end{cases} \tag{3}$$

and where κ_a^α and κ_b^β quantify the chance that the first and the second pulse lead to a photon detection event, respectively. Eq. 2 can be understood as the product of the probabilities (i) that the molecule is excited at time zero, (ii) that it emits a photon at time t', (iii) that the molecule is re-excited by a second pulse at time p, and (iv) that it emits a second photon at time $t'+t$, see also Figure 2. The upper integration limit p is explained by the fact that if the molecule has not emitted a photon until the second excitation pulse, it is still in its excited state, thus cannot be re-excited, and one cannot obtain *two* photons with the two excitation pulses in this case. The values of κ_a^α and κ_b^β depend on the excitation (a,b) and detection (α,β) polarization as well as the consecutive orientations of the molecule's absorption/emission dipole.

The chance to detect two photons with lag time t from two different molecules is similar to Eq. 2, but with the difference that the upper integration limit can now be extended to infinity, leading to

$$\int_{\max(p-t,0)}^{\infty} dt' \frac{\kappa_a^\alpha}{\tau} e^{-t'/\tau} \frac{\kappa_b^\beta}{\tau} e^{-(t'+t-p)/\tau} = \frac{\kappa_a^\alpha \kappa_b^\beta}{2\tau} \exp\left(-\frac{|\,t-p\,|}{\tau}\right) \equiv \kappa_a^\alpha \kappa_b^\beta F_2(t,\tau,p) \tag{4}$$

where the last equation defines the new function $F_2(t,\tau,p)$. The value of $F_1(t,\tau,p)$, in contrast to that of $F_2(t,\tau,p)$, approaches zero when the pulse delay p goes to zero, which is the essence of fluorescence antibunching.

Let us consider the limit of $\tau \to 0$, i.e. when the fluorescence lifetime becomes negligibly small compared with all other times of interest, in particular the inter-pulse distance p and the characteristic rotational diffusion times. This is exactly the situation that will be of interest in Section 4. For $\tau \to 0$ one finds

$$F_1(t,p) = \begin{cases} 0 & p = 0 \\ \delta(t-p) & p > 0 \end{cases} \tag{5}$$

and

$$F_2(t,p) = \delta(t-p) \tag{6}$$

where $\delta(x)$ is Dirac's δ-function. Furthermore, if the excitation is done periodically with repetition period p, the complete time-dependent part of the correlation function takes the simplified form

$$g_{ab}^{\alpha\beta}(t) = \epsilon c \sum_{k=1}^{\infty} \langle \kappa_a^\alpha(t_0) \kappa_b^\beta(t_0+t) \rangle_{t_0} \delta(t-kp) + \epsilon^2 c^2 \langle \kappa_a^\alpha(t_0) \rangle_{t_0} \langle \kappa_b^\beta(t_0) \rangle_{t_0} \sum_{k=0}^{\infty} \delta(t-kp) \tag{7}$$

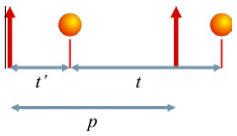

Figure 2. Schematic of the considered two-photon correlation experiment: a first laser pulse (left vertical arrow) excites a molecule, which emits a fluorescence photon (yellow sphere) at time t'. A second laser pulse (right vertical arrow) re-excites the molecule (or excites a second one) at time p, and a second fluorescence photon is emitted at time $t'+t$. Time flow is from left to right.

where c is the concentration of fluorescing molecules, and ϵ takes in all factors related to global excitation and detection efficiency as well as fluorescence quantum yield. The first sum accounts for photon pairs generated by one and the same molecule (and thus enters the correlation function proportionally to ϵc), and the second sum accounts for photon pairs generated by two different molecules (and thus enters the correlation function proportionally to $\epsilon^2 c^2$). The effect of rotational diffusion (i.e. the rotation of absorption/emission dipole) is contained in the pre-factors κ_a^α and κ_b^β or, more precisely, in the joint correlation of these factors that enters the first sum of the last equation. We will consider this rotational-diffusion related part of the correlation function within the next subsections.

2.2. Rotational diffusion

The general theory of rotational diffusion of an anisotropic rotor can be found in several textbooks on quantum mechanics and was, in the context of correlation spectroscopy and light scattering, developed by Aragón and Pecora, [13,3]. Let us start from the rotational diffusion equation

$$\frac{\partial P}{\partial t} = \left(D_a \hat{J}_a^2 + D_b \hat{J}_b^2 + D_c \hat{J}_c^2\right) P \tag{8}$$

where a, b, and c denote the principal axes of rotation of the molecule, $P = P(\psi,\theta,\phi)$ is the probability density to find the molecule's principal axes rotated by Euler angles ψ, θ, and ϕ with respect to the lab frame, the $D_{a,b,c}$ are the generally different rotational diffusion coefficients around the molecule's principal axes, and the $\hat{J}_{a,b,c}$ are the three angular momentum operators around these axes. Eq. 8 is derived analogously to the more familiar translational diffusion equation. The difficulty with Eq. 8 is that the angular momentum operators relate to the intrinsic frame of the molecule's principal axes which is rotating in time with respect to the fixed lab frame. To simplify matters, one can first rotate the molecule back to the lab's frame so that its axes align with the fixed Cartesian coordinate axes of the lab frame, then apply the operator, and finally rotate the molecule back, i.e.

$$\frac{\partial P}{\partial t} = \hat{R}\left(D_a \hat{J}_x^2 + D_b \hat{J}_y^2 + D_c \hat{J}_z^2\right) \hat{R}^{-1} P \tag{9}$$

where $\hat{R}$ denotes the operation of rotating the molecule's frame from an orientation aligned with the lab's Cartesian x,y,z-coordinates to its actual orientation as specified by the Euler angles ψ, θ, and ϕ. The rotation operator $\hat{R}$ can be decomposed into

$$\hat{R} = \hat{R}_z(\phi) \hat{R}_y(\theta) \hat{R}_z(\psi) \tag{10}$$

where $\hat{R}_{y,z}(\beta)$ denotes a rotation by angle β around axis y or z, respectively. The advantage of Eq. 9 is that the angular momentum operators are now referring to the fixed lab frame. To further analyze Eq. 9, let us consider the special case that the function p is replaced by

$$P = \hat{R} \mid \ell, m\rangle \tag{11}$$

where $\mid \ell, m\rangle$ is an eigenfunction of the angular momentum operator obeying the two relations

$$\hat{\mathbf{J}}^2 \mid \ell, m\rangle = (\hat{J}_x^2 + \hat{J}_y^2 + \hat{J}_z^2) \mid \ell, m\rangle = \ell(\ell+1) \mid \ell, m\rangle \tag{12}$$

and

$$\hat{J}_z \mid \ell, m\rangle = m \mid \ell, m\rangle \tag{13}$$

Inserting Eq. 11 into Eq. 9 yields

$$\frac{\partial(\hat{R} \mid \ell, m\rangle)}{\partial t} = \hat{R}\left(D_a \hat{J}_x^2 + D_b \hat{J}_y^2 + D_c \hat{J}_z^2\right) \mid \ell, m\rangle \tag{14}$$

Next, the action of the rotation operator $\widehat{R}$ on $\mid \ell, m\rangle$ is given by (see e.g. [21])

$$\widehat{R}(\phi,\theta,\psi) \mid \ell, m\rangle = \sum_{k=-\ell}^{\ell} D^{\ell}_{km}(\phi,\theta,\psi) \mid \ell, k\rangle \tag{15}$$

where the $D^{\ell}_{km}(\phi,\theta,\psi)$ are Wigner rotation matrices defined by

$$D^{\ell}_{km}(\phi,\theta,\psi) = \exp(ik\phi + im\psi) d^{\ell}_{km}(\theta) \tag{16}$$

and

$$\begin{aligned} d^{\ell}_{km}(\theta) &= \langle \ell, k \mid R_y(\theta) \mid \ell, m\rangle \\ &= \frac{\sqrt{(\ell+k)!(\ell-k)!(\ell+m)!(\ell-m)!}}{k!} \times \sum_n \\ &\quad \times \frac{(-1)^{\ell+k-n} C^{2n-m-k} S^{2\ell+m+k-2n}}{(\ell+m-n)!(\ell+k-n)!(n-m-k)!} \end{aligned} \tag{17}$$

where we have used the abbreviations $C = \cos(\theta/2)$ and $S = \sin(\theta/2)$.

For the sake of simplicity, we will further consider the special case of a symmetric top rotor where one has $D_a = D_b = D_\perp$ and $D_c = D_{||}$. This is also the case of most practical relevance, because real FCS data will rarely allow for discerning more than two non-equal rotational diffusion coefficients. For the symmetric top rotor, one finds, by multiplying Eq. (14) with $\langle \ell, k \mid$, that the functions

$$e^{-\left[D_\perp \ell(\ell+1)+(D_{||}-D_\perp)m^2\right]t} D^{\ell}_{mk}(\phi,\theta,\psi) \tag{18}$$

are eigenfunctions of the rotational diffusion equation. Moreover, Wigner's rotation matrices obey the orthogonality relation

$$\begin{aligned} &\int_0^{\pi} d\theta \sin\theta \int_0^{2\pi} d\phi \int_0^{2\pi} D^{\ell *}_{mk}(\phi,\theta,\psi) D^{\ell'}_{m'k'}(\phi,\theta,\psi) \\ &= \frac{8\pi^2}{2\ell+1} \delta_{\ell,\ell'} \delta_{k,k'} \delta_{m,m'} \end{aligned} \tag{19}$$

where a star, as usual, denotes complex conjugation. The $\delta_{a,b}$ are Kronecker symbols taking the value one for $a = b$ and zero otherwise. With this complete orthogonal system of eigenfunctions, the probability density that a molecule has rotated, within time t, from an initial orientation Ω' described by the Euler angles ϕ', θ' and ψ' into a final orientation Ω described by Euler angles ϕ, θ and ψ is given by Green's function in the standard way as

$$\begin{aligned} G(\Omega,\Omega',t) = \sum_{\ell=0}^{\infty} \sum_{k,m=-\ell}^{\ell} &\frac{2\ell+1}{8\pi^2} D^{\ell}_{km}(\phi,\theta,\psi) \\ &\times D^{\ell *}_{km}(\phi',\theta',\psi') e^{-\left[D_\perp \ell(\ell+1)+(D_{||}-D_\perp)m^2\right]t} \end{aligned} \tag{20}$$

2.3. Excitation and detection

Next, one has to consider the peculiarities of fluorescence excitation and detection. Generally, the absorption and emission dipole of a fluorescent molecule will not be collinear, and we will denote the angle between both by χ. Let us start with orienting the absorption dipole $\mathbf{v}_0$ along the z-axis of the molecular frame, whereas the emission dipole shall be oriented along $\mathbf{w}_0 = \{\sin(\chi), 0, \cos(\chi)\}$. Then, an arbitrary orientation of absorption and emission dipoles is given by

$$\mathbf{v} = \widehat{R}_z(\phi)\widehat{R}_y(\theta)\widehat{R}_z(\psi) \cdot \mathbf{v}_0 \tag{21}$$

$$\mathbf{w} = \widehat{R}_z(\phi)\widehat{R}_y(\theta)\widehat{R}_z(\psi) \cdot \mathbf{w}_0 \tag{22}$$

where the three Euler angles ψ, θ, and ϕ define how the non-collinear emission/absorption dipoles are oriented with respect to the molecule's principal axes. The probability of exciting and detecting a photon from such an orientation of absorption/emission dipoles for a molecule which principal axes are aligned along the coordinate axes of the lab frame and which position is $\mathbf{r}$ is in the most general case proportional to

$$U^{\alpha}_a(\phi,\theta,\psi,\mathbf{r}) = \sum_{p,q,r,s=1}^{3} u_{a,pq}(\mathbf{r}) v_p v_q u^{\alpha}_{rs}(\mathbf{r}) w_r w_s \tag{23}$$

where the ϕ,θ,ψ-dependence on the right hand side is indirectly contained within the vector components of $\mathbf{v}$ and $\mathbf{w}$ via (21) and (22). The functions $u_{a,pq}(\mathbf{r})$ depend on the position-dependent electric field distribution as generated by the focused excitation laser, and the functions $u^{\alpha}_{rs}(\mathbf{r})$ are connected to the peculiarities of the confocal detection, and both have to be calculated for the case that the principal axes of the molecule are parallel to the axes of the lab frame. Remember that the subscript a refers to which excitation laser and the superscript α to which detection channel are used.

Now, we have everything in place for calculating the correlation functions $\langle \kappa^{\alpha}_a(t_0)\kappa^{\beta}_b(t_0+t)\rangle_{t_0}$. These is given by the product of the probability to excite/detect a photon from a molecule at position $\mathbf{r}$ and having orientation Ω with respect to the lab frame, times the probability that it rotates from orientation Ω to orientation Ω' within time t, times the probability to detect a second photon from a molecule at the same position $\mathbf{r}$ but having orientation Ω'. Thus, we find

$$\begin{aligned} \langle \kappa^{\alpha}_a(t_0)\kappa^{\beta}_b(t_0+t)\rangle_{t_0} &= \int d\mathbf{r} \int d\omega \int d\Omega \int d\Omega' U^{\alpha}_a[R(\Omega)\omega,\mathbf{r}] \\ &\quad \times G(\Omega,\Omega',t) U^{\beta}_b[R(\Omega')\omega,\mathbf{r}] \\ &= \int d\mathbf{r} \int d\omega \int d\Omega \int d\Omega' \left[R^{-1}(\Omega) U^{\alpha}_a(\omega,\mathbf{r})\right] \\ &\quad \times G(\Omega,\Omega',t) \left[R^{-1}(\Omega') U^{\beta}_b(\omega,\mathbf{r})\right] \end{aligned} \tag{24}$$

where the integrations extend over all possible initial and final orientations Ω and Ω' of a molecule, over all orientations ω of the absorption/emission dipoles with respect to the to molecular frame, and over all possible positions $\mathbf{r}$ of a molecule within the sample. Here we have to important assumptions: Firstly, a molecule does not move during the considered time t, i.e. rotational diffusion is by orders of magnitude faster than the typical lateral diffusion time of a molecule through the detection volume; and secondly, that we average over all possible orientations of the absorption/emission dipole with respect to the molecular frame. This last assumption is reasonable for non-specific random labeling of macromolecules.

Because Wigner matrices constitute a complete orthogonal function system, the functions $U^{\alpha}_a(\mathbf{r})$ can be expanded into the series

$$U^{\alpha}_a(\phi,\theta,\psi,\mathbf{r}) = \tag{25}$$

$$\sum_{\ell=0}^{\infty} \sum_{k,m=-\ell}^{\ell} \sqrt{\frac{2\ell+1}{8\pi^2}} (u^{\alpha}_a)^{\ell}_{km}(\mathbf{r}) D^{\ell}_{km}(\phi,\theta,\psi)$$

where the $(u^{\alpha}_a)^{\ell}_{km}(\mathbf{r})$ are the position dependent expansion coefficients not to be confused with the excitation and detection coefficients, $u_{a,pq}(\mathbf{r})$ and $u^{\alpha}_{pq}(\mathbf{r})$, in Eq. (23). These expansion coefficients can be explicitly calculated by

$$\begin{aligned} (u^{\alpha}_a)^{\ell}_{km}(\mathbf{r}) = \sqrt{\frac{2\ell+1}{8\pi^2}} &\int_0^{\pi} d\theta \sin\theta \int_0^{2\pi} d\phi \\ &\times \int_0^{2\pi} d\psi D^{\ell *}_{km}(\phi,\theta,\psi) U(\phi,\theta,\psi,\mathbf{r}) \end{aligned} \tag{26}$$

Because the $U^{\alpha}_a(\mathbf{r})$ are fourth order polynomials of the components of the absorption and emission dipole vectors, the maximum value of ℓ yielding non-zero coefficients is four. Thus, there can be

at maximum $\sum_{\ell=0}^{4}(2\ell+1)=15$ independent non-zero coefficients in the above series expansion. Due to symmetry reasons, the actual number will be even smaller. To simplify matters further, one can use the transformation relation of Wigner matrices

$$[R_z(\alpha)R_y(\gamma)R_z(\beta)D]^{\ell}_{km}(\phi,\theta,\psi)=\sum_j D^{\ell}_{kj}(\alpha,\gamma,\beta)D^{\ell}_{jm}(\phi,\theta,\psi) \tag{27}$$

Inserting Eqs. (25) and (20) into Eq. (24), using relations (19) and (27), and carrying out all integrations, one finally obtains the compact result

$$\langle\kappa^{\alpha}_a(t_0)\kappa^{\beta}_b(t_0+t)\rangle_{t_0}=\sum_{\ell=0}^{4}\sum_{m=-\ell}^{\ell}(f^{\alpha\beta}_{ab})^{\ell}_m e^{-\left[D_{\perp}\ell(\ell+1)+(D_{\parallel}-D_{\perp})m^2\right]t} \tag{28}$$

where we have introduced the abbreviation

$$(f^{\alpha\beta}_{ab})^{\ell}_m=\sum_{k=-\ell}^{\ell}\int d\mathbf{r},(u^{\alpha}_a)^{\ell}_{mk}(\mathbf{r})(u^{\beta}_b)^{\ell*}_{mk}(\mathbf{r}) \tag{29}$$

Thus, the whole problem condenses to determining the coefficients $(f^{\alpha\beta}_{ab})^{\ell}_m$ by first calculating the explicit excitation/detection alias molecule detection function, Eq. (23), via standard wave-optics, next to find the coefficients $(u^{\alpha}_a)^{\ell}_{km}(\mathbf{r})$ via Eq. (26), and finally to calculate $(f^{\alpha\beta}_{ab})^{\ell}_m$ by integrating over $\mathbf{r}$ in the last equation.

As reference we will consider the case of an optics with negligibly small numerical aperture, so that excitation and detection is done by plane waves. In practice, such an experiment cannot be realized because the detection volume would become infinitely large. For this plane-wave reference, the coefficients $(f^{\alpha\beta}_{ab})^{\ell}_m$ can be calculated analytically by setting $u_{a,pq}(\mathbf{r})=\delta_{ap}\delta_{aq}\delta(\mathbf{r})$ and $u^{\alpha}_{rs}(\mathbf{r})=\delta_{\alpha p}\delta_{\alpha q}\delta(\mathbf{r})$ in Eq. (25) (assuming collinear absorption/emission dipoles). All resulting non-zero coefficients $(f^{\alpha\beta}_{ab})^{\ell}_m$ are listed in Table 1, where the indices $\parallel$ and $\perp$ indicate polarization of excitation/detection along two orthogonal directions as shown in Figure 1. In that table, we omitted the coefficients with $\ell=0$ and $m=0$, which contribute only to a constant offset in the correlation curve and thus do not carry any information about the rotational diffusion.

In general, there exist 16 correlation function for all possible combinations of excitation and detection polarizatons of the first and second photon. However, for symmetry reasons there are only four distinct correlation curves, which are $g^{\parallel\parallel}_{\parallel\parallel}=g^{\perp\perp}_{\perp\perp}$, $g^{\parallel\perp}_{\parallel\parallel}=g^{\perp\parallel}_{\perp\perp}=g^{\perp\parallel}_{\parallel\parallel}=g^{\parallel\parallel}_{\perp\perp}=g^{\parallel\perp}_{\parallel\perp}=g^{\perp\perp}_{\perp\parallel}=g^{\parallel\parallel}_{\perp\parallel}=g^{\perp\perp}_{\parallel\perp}$, $g^{\perp\perp}_{\parallel\parallel}=g^{\parallel\parallel}_{\perp\perp}=g^{\parallel\perp}_{\perp\parallel}=g^{\perp\parallel}_{\perp\perp}$, and $g^{\parallel\perp}_{\perp\parallel}=g^{\perp\parallel}_{\perp\parallel}$. It is important to notice that only correlation curves with the same two subscripts are measurable in conventional FCS experiments, where excitation is done with only one linearly polarized laser. All correlation curves with a pair of different subscripts can be measured only with a set-up employing pulsed interleaved excitation (PIE) [22], where two lasers with orthogonal polarization are pulsed alternatively in rapid succession so that one has indeed the chance to detect photon pairs where the two photons resulted from excitation events with two different and orthogonal polarizations. We will call the resulting FCS measurement scheme PIE-FCS.

Table 1
Values of coefficients $(f^{\alpha\beta}_{ab})^{\ell}_m$ for plane wave excitation and detection and collinearity of absorption and emission dipole. All values are normalized by $(f^{\parallel\parallel}_{\parallel\parallel})^2_0$.

$(f^{\parallel\parallel}_{\parallel\parallel})^{\ell}_m$	$m=0$	$m=\pm2$	$m=\pm4$
$\ell=2$	1	3/2	0
$\ell=4$	1/20	1/18	7/72
$(f^{\parallel\perp}_{\parallel\parallel})^{\ell}_m$	$m=0$	$m=\pm2$	$m=\pm4$
$\ell=2$	1/3	0	0
$\ell=4$	1/60	0	−7/72
$(f^{\perp\perp}_{\parallel\parallel})^{\ell}_m$	$m=0$	$m=\pm2$	$m=\pm4$
$\ell=2$	1/9	0	0
$\ell=4$	1/180	0	7/72
$(f^{\parallel\perp}_{\parallel\perp})^{\ell}_m$	$m=0$	$m=\pm2$	$m=\pm4$
$\ell=2$	1	−3/2	0
$\ell=4$	1/20	−1/18	7/72

2.4. Rotational diffusion and molecular shape

The rotational diffusion of any object can be described by that of an ellipsoid with three orthogonal axes of rotation (principal axes). In almost all cases of practical interest, it is sufficient to approximate a molecule by an ellipsoid of rotation, i.e. an ellipsoid that has two identical rotational diffusion constants around two of its principal axes and one different around the third (symmetry axis). This is equivalent to approximating the shape of a molecule by a prolate or oblate ellipsoid of rotation. Following Perrin [23,24] and Koenig [25], the rotational diffusion coefficients for an prolate ellipsoid of rotation with aspect ratio $\kappa=R_{\perp}/R_{\parallel}<1$ are given by

$$\frac{D_{\perp}}{D_0}=\frac{3\kappa^2}{2(1-\kappa^4)}\left\{\frac{2-\kappa^2}{\sqrt{1-\kappa^2}}\ln\left[\frac{1+\sqrt{1-\kappa^2}}{\kappa}\right]-1\right\} \tag{30}$$

and

$$\frac{D_{\parallel}}{D_0}=\frac{3}{2(1-\kappa^2)}\left\{1-\frac{\kappa^2}{\sqrt{1-\kappa^2}}\ln\left[\frac{1+\sqrt{1-\kappa^2}}{\kappa}\right]\right\} \tag{31}$$

whereas for a oblate ellipsoid of rotation ($\kappa>1$) they read

$$\frac{D_{\perp}}{D_0}=\frac{3\kappa^2}{2(1-\kappa^4)}\left\{\frac{2-\kappa^2}{\sqrt{\kappa^2-1}}\arctan\left(\sqrt{\kappa^2-1}\right)-1\right\} \tag{32}$$

and

$$\frac{D_{\parallel}}{D_0}=\frac{3}{2(1-\kappa^2)}\left\{1-\frac{\kappa^2}{\sqrt{\kappa^2-1}}\arctan\left(\sqrt{\kappa^2-1}\right)\right\} \tag{33}$$

Here, D_0 is the diffusion coefficient of a sphere of radius R_0 with the same volume as the ellipsoid, i.e. $R_0^3=R_{\parallel}R_{\perp}^2$, and the value of D_0 is given by the Stokes–Einstein–Debye equation

$$D_0=\frac{k_BT}{8\pi\eta R_0^3} \tag{34}$$

where k_B is Boltzmann's constant, T the absolute temperature, and η the solvent's viscosity. In all the above expressions, the subscript $\parallel$ refers to the symmetry axis, and the subscript $\perp$ to the two transversal axes of the ellipsoid.

3. Numerical explorations

In this section, we will use the general theory as expanded in the previous section for modeling an actual FCS measurement using the experimental setup as shown in Figure 1. We assume that the system uses a water immersion objective with 1.2 numerical aperture and 3 mm focal distance for focusing and detecting light; that measurements are performed in a solution having the refractive index of water (perfect refractive index matching); that the pinhole radius of the confocal aperture is equal to 75 μm; that magnification at the plane of the confocal aperture is 60 times; and that excitation and center emission wavelengths are 640 nm and 670 nm, respectively. When knowing all these parameters, the exact molecule detection function (product of excitation intensity distribution with detection efficiency function) can be calculated in standard way, using the classical work by Richards and Wolf for calculating the transmission of electromagnetic waves through an optical system with large numerical aperture [26,27]. We performed these calculations for all possible combinations of

excitation and detection polarization, thus obtaining the $U_a^{\alpha}(\mathbf{r})$ of Eq. (23). From these functions, the coefficients $(f_{ab}^{\alpha\beta})_m^{\ell}$ are calculated as indicated at the end of Section 2.3. In what follows, we will consider the impact of several effects on the performance of an FCS experiment, in particular: depolarization due to the large numerical aperture of the objective (which is necessary for achieving tight focusing and high detection efficiency); non-collinearity of absorption and emission dipoles; shape anisotropy of molecules; and labeling specificities.

3.1. What is the effect of depolarization?

When focusing linearly polarized light with an objective of high numerical aperture into a tight focus, the polarization distribution within the focus will no longer be homogeneous nor linear, see Figure 3. The partially elliptic polarization leads to generally non-vanishing coefficients $u_{a,pq}(\mathbf{r})$ with $p \neq q$ in Eq. (23). Also, the polarization of the fluorescence light collected with such an objective will be mixed, leading similarly to non-vanishing non-diagonal 'detection' coefficients $u_{rs}^{\alpha}(\mathbf{r})$.

When performing an FCS experiment with linearly polarized excitation beam and polarization-sensitive detection, the question arises how much this depolarization changes the measured correlation curves.

As an example, Figure 4 plots the four distinct correlation curves for an isotropic rotor with 40 Å radius (solvent water at 20 °C). This figure shows only the time dependent part of the correlation curve, with any constant offset subtracted. The positively valued curves are accessible by a conventional FCS measurement, whereas the negatively valued curve which exhibits an anti-correlation behavior is only accessible with PIE.

To assess the impact of depolarization we calculated ideal correlation curve for different focusing of the exciting laser beam and fitted these curves globally with the plane-wave reference curves. The free fit parameters were the radius of the isotropic rotor, and the four amplitudes of the correlation curves. The fit procedure uses a Marquardt–Levenberg simplex algorithm for fitting the radius value, and a linear least-square fit for fitting the amplitude values. Figure 5 shows the relative error of determining the radius of the rotor which is made when fitting the correlation curves obtained for different focus radii with a model that completely neglects excitation/detection depolarization by the objective (plane-wave limit). The error made is remarkably small, even for the strongest focusing (diffraction limit), and will be usually much smaller than the intrinsic error introduced by a measurement's photon shot noise. It is important to understand why the fit is so insensitive to depolarization effects: although they change the relative amplitudes of the four correlation curves, they only marginally influence their temporal behavior. Thus, leaving the amplitude values free during fitting is the condition for safely neglecting depolarization effects when analyzing experimental data.

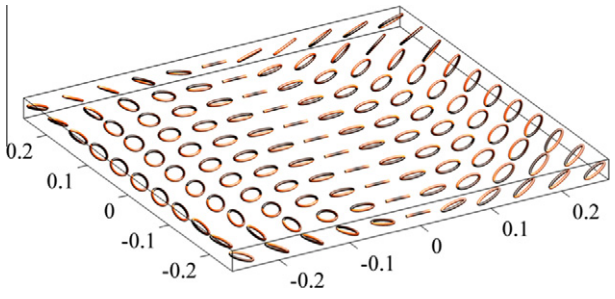

Figure 3. Electric field polarization of the excitation light in the focal plane when focusing a linearly polarized laser (polarization along x-axis) through an objective with 1.2 numerical aperture into a diffraction-limited spot. If **a** and **b** denote the two half-axes of each ellipse, the electric field at the corresponding location is proportional (up to a constant complex number) to $\mathbf{a} + i\mathbf{b}$. Along the line $x = 0$, the field is linearly polarized, so that the ellipses collapse into lines.

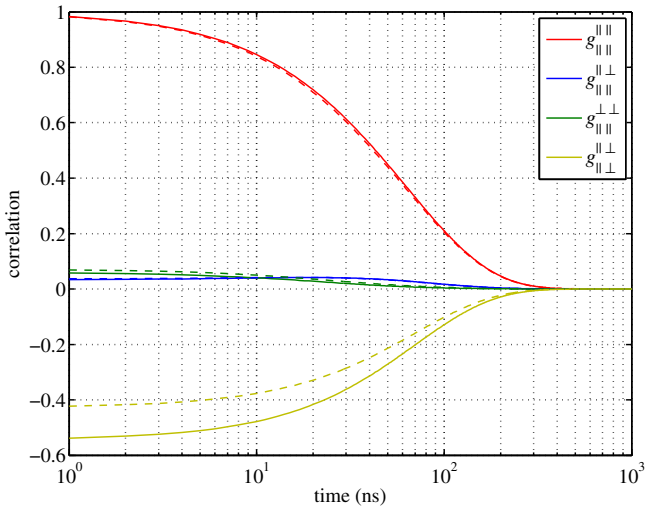

Figure 4. Ideal correlation curves for an isotropic rotor with 40 Å radius in water at 20 °C. Solid lines show correlation curves for the case of maximum focusing ($1/e^2$-beam waist radius in focus is 230 nm), the broken lines show correlation curves in the plane-wave limit. Curves are normalized by the maximum value of the $g_{\parallel\parallel}^{\parallel\parallel}$-correlation.

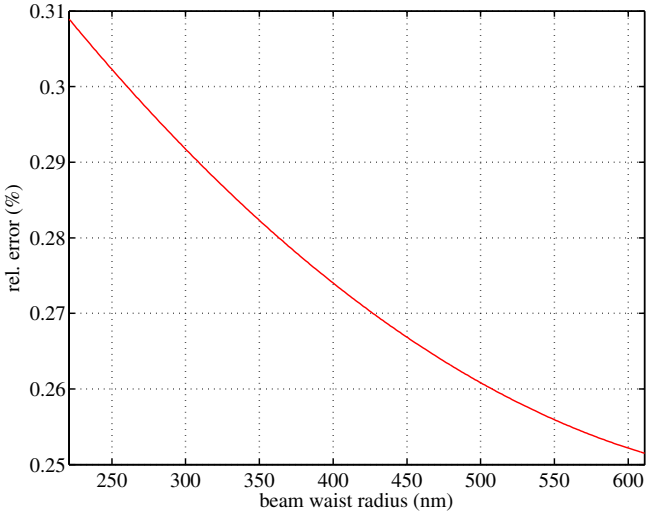

Figure 5. Relative error in determining the radius of an isotropic rotor when fitting correlation curves with a model that neglects depolarization effects.

3.2. What is the effect of non-collinearity between excitation/emission dipole?

For most organic dyes, the absorption and emission dipoles are not exactly collinear. For most fluorescence spectroscopy methods, this is of no concern, but for fluorescence anisotropy or polarization-resolved FCS measurements, one has to take into account that such a non-collinearity rotates the emission polarization with respect to the excitation polarization. Figure 6 shows the difference in the correlation curves for collinear and non-collinear dipoles (25° angle between dipoles).

To study the impact of this effect on the data evaluation of an FCS measurement, we calculated correlation curves for angles

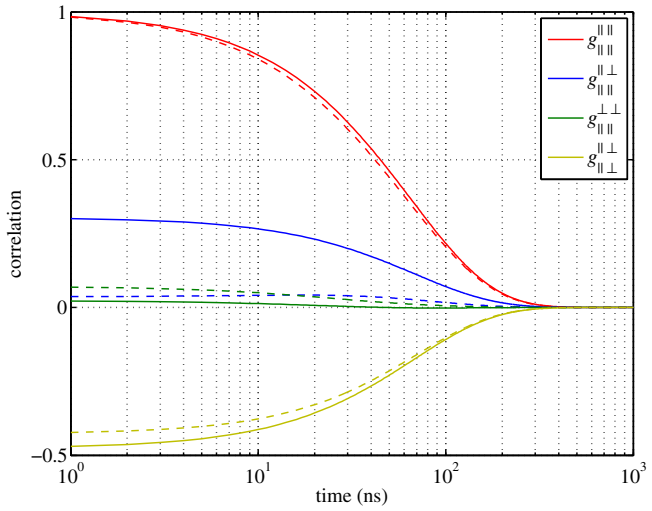

Figure 6. Ideal correlation curves for an isotropic rotor with 40 Åradius in water at 20 °C. Solid lines show correlation curves for the case of non-collinear absorption and emission dipole with an angle of 25° between them, the broken lines show correlation curves for collinear dipoles. All curves are calculated in the plane-wave limit, and normalized by the maximum value of the $g_{\parallel\parallel}^{\parallel\parallel}$-correlation.

between absorption and emission dipoles in the range from 0° up to 25°, and globally fitted these curves with model curves obtained for collinear dipoles. Fit parameters were again the radius of the isotropic rotor, and the amplitudes of the correlation curves. The resulting relative error in the resulting radius value is plotted in Figure 7. As can be seen, the made error is negligibly small, even for rather large angles close to 25°, although the small-amplitude correlation curves, $g_{\parallel\parallel}^{\parallel\perp}$ and $g_{\parallel\parallel}^{\perp\perp}$, change considerably with increasing angle between dipoles. This can be explained by the fact that their impact on the global fit quality is rather small due to their small amplitude compared with the two other correlation curves, $g_{\parallel\parallel}^{\parallel\parallel}$ and $g_{\parallel\perp}^{\parallel\perp}$. Another important point to remember is that the absolute amplitudes of the correlation curves do not play any role for fitting the radius value: the amplitudes are free fit parameters themselves, so that the fitted radius value depends only on the *shape* of the curves. Thus, one can safely ignore effects of non-collinearity between absorption and emission dipoles when aiming at determining correct hydrodynamic radius values from FCS measurements of rotational diffusion.

3.3. Is it possible to extract a shape factor from an FCS measurement?

Until now, we have presented numerical calculations only for isotropic rotors. Their is the exciting question whether it is possible to extract, from rotational diffusion measurements, correct information about non-sphericity of the rotor. Let us consider the example a molecule having the shape of an oblate ellipsoid of rotation with 20 Å radius along the symmetry axis and 40 Å along the two orthogonal axes. First, we assume that the FCS measurement is performed in an conventional set-up without PIE, so that only the positively valued correlation curves are available. Figure 8 shows a global fit of these curves using an isotropic rotor model. As can bee seen, the fit quality is nearly perfect, showing that even in the case of an 1:2 aspect ratio it is rather impossible to distinguish between an isotropic rotor and an ellipsoid of rotation on the basis of these FCS data.

The situation improves if one is able to use all four possible correlation curves. This is demonstrated in Figure 9 where again the correlation curves are fitted with an isotropic-rotor model. Now,

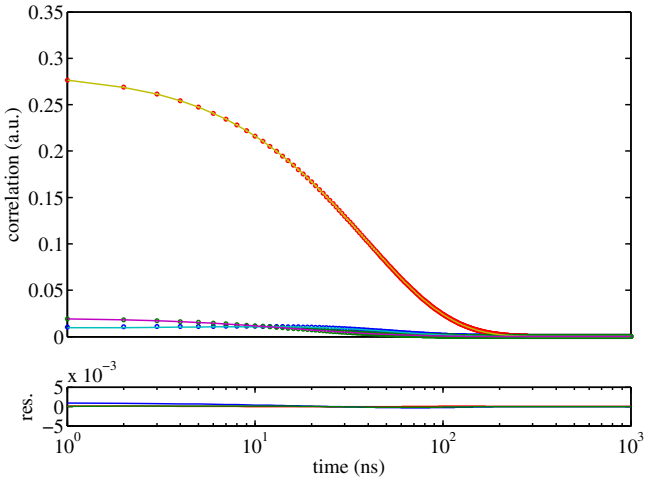

Figure 8. Fit quality when fitting the correlation curves of an anisotropic rotor (symmetry axis 20 Å, orthogonal axes 40 Å) accessible by a conventional FCS measurement with an isotropic-rotor model.

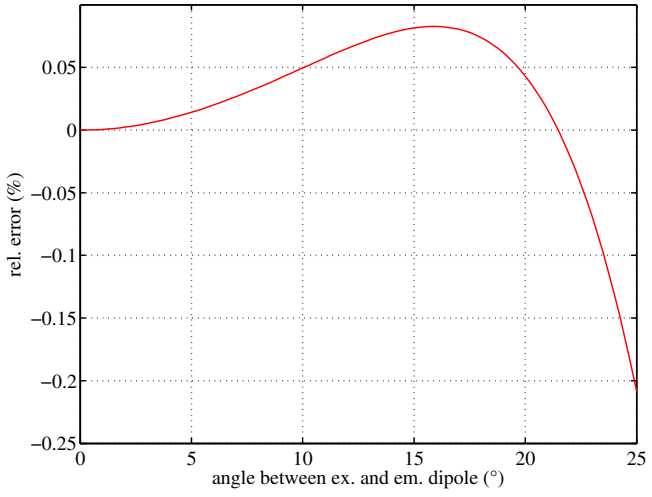

Figure 7. Relative error in determining radius of an isotropic rotor when fitting an ideal measurement curve with a model that assumes collinearity between absorption and emission dipole.

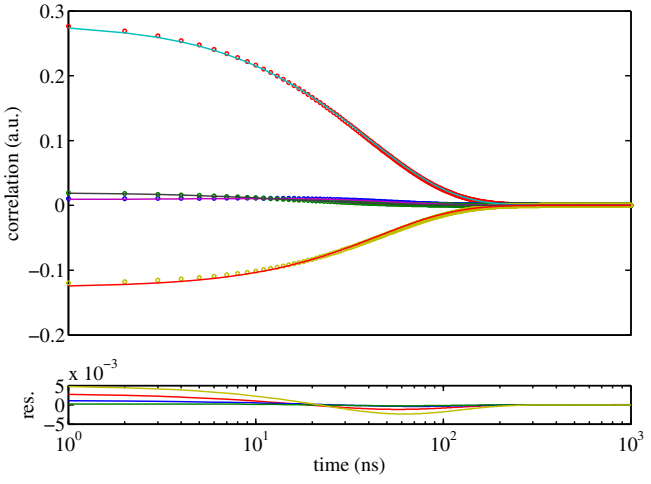

Figure 9. Fit quality when fitting all four possible correlation curves of an anisotropic rotor (symmetry axis 20 Å, orthogonal axes 40 Å) with an isotropic-rotor model.

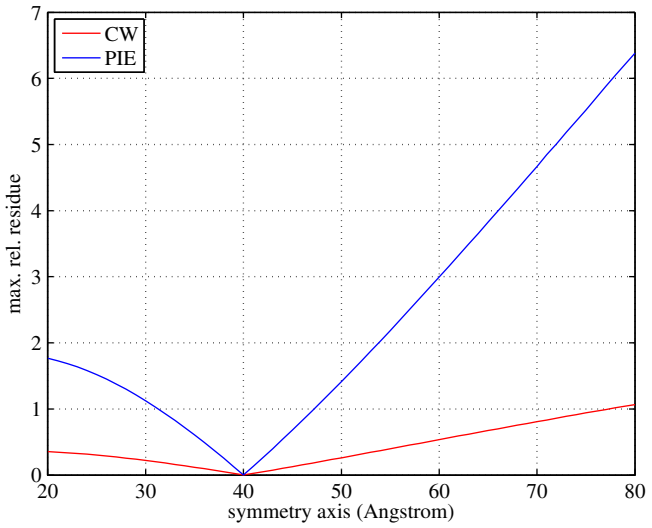

Figure 10. Maximum residual values in percent when fitting the cw-accessible (red) and all four (blue) correlation curves with an isotropic rotor model as a function of the radius value along the symmetry axis of the ellipsoid of rotation. Radius values of orthogonal axes are kept at 40 Å.

the poor fit quality indicates that the isotropic-rotor model does not perfectly describe the 'observed' correlation.

To better quantify this statement for a continuous range of aspect-ratio values, we performed model calculations for aspect-ratio values between 0.5:1 through 2:1 (ratio of radius of symmetry axes to radius of orthogonal axes). The result is shown in Figure 10, where the maximum relative residual of the fit is plotted as function of the radius of the symmetry axis. The maximum relative residual is defined as the maximum absolute difference between all correlation curves and their best fits divided by the maximum absolute value of all correlation curves. As can be seen, the fit quality is ca. 4–5 times more sensitive to the anisotropy of the rotor when using all four possible correlation curves than when using only the positively valued correlation curves. The conclusion is that, by using a conventional FCS measurement set-up which can measure only the positively valued correlation curves, it is rather improbable that one is able to decide, on the basis of the fit quality, whether the underlying rotation diffusion stems from an isotropic or anisotropic rotor, whereas the full set of all four possible correlation curves may indeed offer a chance to measure the shape of a molecule within the limitations of an ellipsoid-of-rotation model.

3.4. What is the effect of label stoichiometry?

Up to now, we have silently assumed that the rotating molecule is connected with one and only one dipolar fluorescence label. In practice, when non-specifically labeling macromolecules such as large proteins, that should not always be the case, although one can always aim at labeling a protein with low label stoichiometry. If there is more than one emitter on the same molecule, and if they have fixed relative orientation, this can severely skew the observed correlation curves. However, this problem is alleviated if one assumes that the relative orientation the emitters on one molecule is randomly changing from molecule to molecule. Let us consider the case of K emitters per molecule. Then, one has to replace in Eq. (7) the correlator $\langle \kappa_a^\alpha(t_0)\kappa_b^\beta(t_0+t)\rangle_{t_0}$ by

$$\left\langle \left(\sum_{s=1}^{K} {}^s\kappa_a^\alpha(t_0)\right)\left(\sum_{s'=1}^{K} {}^{s'}\kappa_b^\beta(t_0+t)\right)\right\rangle_{t_0} \tag{35}$$

where the left upper superscripts s and s' refer to the different emitters on one molecule. Thus, additionally to the 'diagonal' correlation terms with $s = s'$, there appear also 'non-diagonal' correlation terms with $s \neq s'$. However, if the relative orientation of the emitters is randomly changing from molecule to molecule, than averaging over all molecules with all possible relative orientations of their emitters leads to a factorization of the correlation, i.e.

$$\langle\langle {}^s\kappa_a^\alpha(t_0)\,{}^{s'}\kappa_b^\beta(t_0+t)\rangle\rangle_{t_0} = \langle\langle {}^s\kappa_a^\alpha(t_0)\rangle\rangle_{t_0}^2 = \text{const.} \tag{36}$$

where the double angular brackets now indicate averaging over all molecules *and* start times t_0. Thus, as long as labeling is done completely randomly and with no intrinsic statistical correlation between emitter orientations on the same molecules, these non-diagonal correlation terms do not contribute to the time-dependent part of the correlation functions.

3.5. What is the effect of label orientational flexibility?

Last but not least, one has to consider the effect of a possible orientational flexibility of the fluorescent labels on the labeled macromolecule. When labeling macromolecules with dyes using standard labeling chemistry, they are typical linked to the macromolecule with a flexible linker. If the used dye is sufficiently hydrophobic and finds sufficiently hydrophobic patches on the macromolecule's surface, it can rigidly attach to the molecule and will co-rotate with it. However, in most cases this will not be the case: the attached dye will be flexibly attached and will exhibit fast rotational diffusion by its own, although, probably, with some orientational restriction. Typical rotational diffusion times of dye molecules in aqueous solutions are on the order of some hundred picoseconds, thus by orders of magnitude faster than the rotation diffusion times of large proteins or DNA/RNA molecules, so that one will not observe any correlation decay on the time scale of the rotational diffusion of the labeled macromolecule if the label is free to rotate on its anchor point. For measuring the rotational diffusion coefficients of the tagged macromolecule, it is necessary to assure rigid co-rotation of the label, which can be achieved by using bis-functional dyes that can bind at both ends to a macromolecule. Even then, slight wobbling of the label can be possible. However, this is similar to the situation of non-collinear excitation and emission dipoles, and as we have seen above, such non-collinearity has negligible impact on the fit results.

4. Experimental case study: aldolase

In this section we will exemplify the measurement of rotational diffusion coefficients and thus size and shape of a macromolecule on the example rabbit muscle aldolase, the structure of which is known from X-ray crystallography (code 1zah in the Brookhaven Protein Data Bank). The next subsection briefly describes the experimental set-up which is needed for measuring *all* possible correlation curves. Then, we discuss the procedure that is used for calculating the correlation curves from the measured single-photon data. The third sub-section gives information about the used dye and labeling procedure, and the final subsection presents the experimental results on the rotational diffusion of aldolase.

4.1. Measurement set-up

The principal measurement set-up used for the experimental work was already depicted in Figure 1. It is a commercial confocal microscopy system (MicroTime 200 with dual-focus option, PicoQuant GmbH, Berlin, Germany) which is similar to the set-up described in detail in Ref. [2]. In summary, the light of two identical, linearly polarized pulsed diode lasers (wavelength 640 nm, pulse duration 50 ps fwhm) is combined by a polarizing beam splitter. Both lasers are pulsed synchronously with a

repetition rate of 80 MHz. A delay of half the repetition period between the two pulse trains of the first and second laser was introduced by inserting an additional cable of appropriate length between the laser driver and the second laser diode. The cw-power of the lasers had been adjusted to 400 μW each. Both beams are coupled into a polarization-maintaining single mode fiber. At the fiber output, the light is collimated and reflected by a dichroic mirror towards the microscope's objective (UPLSAPO 60 × W, 1.2 N.A., Olympus Deutschland GmbH, Hamburg, Germany).

Fluorescence is collected by the same objective (epi-fluorescence setup), passed through the dichroic mirror, and focused onto a single circular aperture (diameter 150 μm). After the pinhole, the light is collimated, split first by a polarizing beam splitter and then by two 50/50 beam splitters, and focused onto four single-photon avalanche diodes (two SPCM-AQR-13, PerkinElmer Optoelectronics, Wiesbaden, Germany, and two MPDs, Bolzano, Italy). A single-photon counting electronics (HydraHarp 400, PicoQuant GmbH, Berlin, Germany) records the detected photons of all four detectors independently with an absolute temporal resolution of two picoseconds on a common time frame. Due to the dead-time of approximately 150 ns of the avalanche diodes after a photon detection event, using four detector is necessary if one is interested in recording all possible combinations of excitation and detection polarization.

All measurements were done in Lab-Tek II chambered coverglass systems (Nunc Thermo Electron LED GmbH, Langenselbold, Germany) coated with BSA to prevent unspecific adsorption of the labeled protein. Sample temperature was controlled with a HH500 digital thermometer (Omega Newport Electronics GmbH, Deckenpfronn, Germany).

4.2. Calculation of correlation curves

Excitation is done in PIE mode (PIE-FCS) with laser pulses of approximately 50 ps duration and an inter-pulse distance of 6.25 ns. The fluorescence decay time of the used label is around 1 ns, so that the fluorescence generated by one pulse has nearly completely decayed when the next excitation pulse arrives. As described above, photon detection is done on an absolute time scale and common time frame for all detectors with a temporal resolution of 2 ps. Thus, by evaluating the arrival times of the detected photons with respect to the pulse train generated by the excitation lasers, one can unequivocally correlate each photon with the laser pulse that excited it, and thus with the corresponding excitation polarization. Moreover, because each detected photon is also correlated with the detector that recorded it, the detection polarization for each photon is known.

Using this information, all 16 possible correlation curves can be calculated using a dedicated correlation software for converting asynchronous single-photon data into correlation curves. The details of this algorithm have described before, and the reader is referred to Ref. [30].

4.3. Fluorescent labeling

As emphasized in the theory section, one pre-requisite for a successful measurement of the rotational diffusion of a macromolecule is the rigid co-rotation of the fluorescent label with the macromolecule. Conventional labeling techniques using monofunctional dyes with a maleiimide reactive group for cysteine labeling or a NHS-ester group for amino labeling, will usually not guarantee that the attached dye is rigidly co-rotating with the labeled entity. Fortunately, several bis-functional dyes are available that exhibit two reactive NHS-ester groups. With these dyes, proteins can be non-specifically labeled via their amino-group containing lysins. Most large proteins expose sufficiently large numbers of lysin residues on their surface that enable rigid and random labeling.

For successfully applying the PIE scheme, it is important that the fluorescence lifetime of the used label is much shorter than the PIE-pulse distance, in our case 6.25 ns. This is true for the commercially available bis-functional dyes Cy5 (1 ns) and Cy3 (0.3 ns). Due to lower background in the red spectral region, and higher quantum yield, Cy5 is the more recommendable label. Thus, aldolase was labeled with Cy5 bis-succinimidyl ester (GE Healthcare Europe GmbH, Freiburg, Germany), then purified using an HPLC system (Jasco Labor und Datentechnik GmbH, Groß-Umstadt, Germany), kept in phosphate buffered saline (PBS) at pH 7.4, and was used for measurements directly after preparation.

4.4. Results

The total measurement time was 5 h. Correlation curves were then calculated between 6 ns and 5 μs lag time. By excluding the zero lag-time value, one eliminates any fluorescence antibunching effect. When analyzing the curves, one has to take into account also the photo-physics of Cy5, comprising both of a light induced switching between a fluorescent trans and a non-fluorescent cis-conformation, and of inter-system crossing between singlet and triplet states.

As a result, two characteristic mono-exponential decays are observed in the correlation functions, one slow with ca. 2 μs decay time, and one fast with ca. 170 ns decay time. We first fitted the correlation functions within the lag-time range between 1 and 5 μs (where all contributions from the rotational diffusion are already decayed) with mono-exponential decay curves having the same decay time, and subtracted these curves from the full correlation functions. The result is shown by circles in Figure 11.

The reduced correlation curves were then fitted in five different ways: (A) using only the positively valued correlation curves and assuming an isotropic-rotor model, neglecting depolarization effects and assuming collinear absorption/emission dipoles; (B) using all correlation curves and assuming an isotropic-rotor model, again neglecting depolarization effects and assuming collinear absorption/emission dipoles; (C) using all correlation curves and assuming an ellipsoid-of-rotation model; again neglecting depolarization effects and assuming collinear absorption/emission dipoles; (D) using all correlation curves and assuming an ellipsoid-of-rotation model, but now taking into account depolarization effects by the objective ($1/e^2$-radius of excitation focus

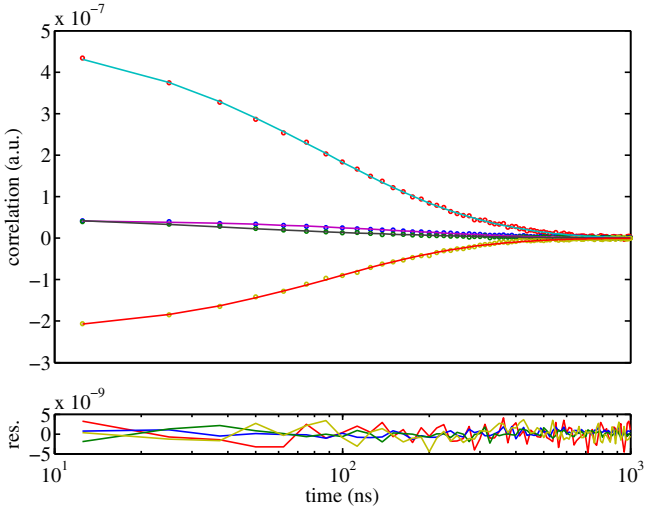

Figure 11. FCS measurement result for aldolase (circles). Solid lines show fit result with an anisotropic rotor model.

was a priori measured to be 350 nm) but keeping absorption/emission dipoles collinear; (E) using all correlation curves, assuming an ellipsoid-of-rotation model, and taking into account depolarization effects and setting the angle between absorption and excitation dipole to 5° (the approximate angle between excitation and emission dipole for Cy5, see Ref. [28]). For satisfactorily fitting the correlation curves, we had to include an additional mono-exponential decay into the correlation, which takes care of the fast photo-physical relaxation of Cy5 [29]. For determining error estimates of the fit values, we used a bootstrap approach: we calculated correlation curves for measurement durations of 30 min, thus generating 10 sets of correlation curves for the total measurement time of 5 h. Next we chose randomly five of these sets, added the corresponding correlation curves, and fitted them. We repeated this procedure 100 times, each time choosing randomly 5 sets of correlation curves out of the 10 sets. The errors of the fit values were then estimated as the standard deviation of the recorded fit results.

The fit results are compared in Table 2. The last column indicates the fit quality by presenting the maximum relative value of the residuals, as already described in Section 3.3. Although the fit quality is only slightly different for the different approaches, it is remarkable that it is best for approach (A), which again emphasizes that one has rather no chance to elucidate anisotropic rotational diffusion in a conventional FCS experiment. However, using all four correlation curves helps to check that an ellipsoid-of-rotation model fits the data better than an isotropic-rotor model, as can be seen by the slight improvement in fit residuals. That the different fit residuals do not differ as strongly as shown in Figure 10 is due to the fact that they are dominated by the photon shot noise entering the measured correlation curves and not by the differences between isotropic and anisotropic rotational diffusion. The determined value of the fast photo-physical relaxation time around 170 ns perfectly matches previously reported values for Cy5 under similar excitation intensities [29].

To check how reasonable the fitted radius values of the ellipsoid of rotation are, we overlaid the shape of that ellipsoid with known X-ray structure of the protein, after centering and aligning the principal axes of the ellipsoid with the principal axes of the molecule. The result is shown in Figure 12 which demonstrates visually that the found ellipsoid of rotation approximates reasonably well the actual molecular shape.

Table 2
Results of the FCS data fitting. First column: indicates which kind of data fitting was applied; (A) fit with an isotropic rotor model, using only the correlation curves accessible with a cw-measurement; (B) Fit with an isotropic rotor model, using all four correlation curves; (C) Fit with a rotational ellipsoid model while neglecting depolarization by the high-NA objective and assuming collinearity between dye absorption and emission dipole; (D) Same as C, but taking depolarization effects into account for a focal $1/e^2$-radius of 350 nm; E: same as D, but assuming an angle between absorption and emission dipole of 10°. Second column: radius value of the symmetry axis of the rotational ellipsoid (for isotropic rotor, the sphere radius is given in the next column). Third column: radius value of orthogonal axes of rotational ellipsoid. Fourth column: photophysics relaxation time. Fifth column: maximum relative residual of fit.

	R_1 (Å)	R_2 (Å)	τ_{iso} (ns)	max res. (%)
A	–	39.5 ± 0.8	166 ± 33	1.3
B	–	41 ± 1	173 ± 18	1.6
C	19.8 ± 0.5	48 ± 1	170 ± 8	1.4
D	19.7 ± 0.6	48 ± 2	168 ± 16	1.4
E	19.8 ± 0.6	48 ± 2	169 ± 16	1.4

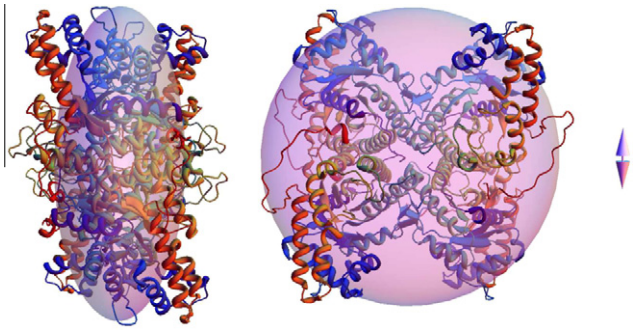

Figure 12. Overlay of aldolase structure as determined from X-ray scattering with rotational ellipsoid as determined with FCS. Left: view along the one of the two long ellipsoid axes. Right: view along the short rotational symmetry axis of the ellipsoid. Double arrow has 1 nm length.

5. Conclusion

We have presented a detailed overview of how to use FCS for measuring the rotational diffusion of macromolecules. We have systematically analyzed all possible sources of systematic errors and found that most of them, such as depolarization effects by high-N.A. objectives, non-collinearity between excitation/emission dipoles, label stoichiometry, or label flexibility, have mostly negligible effect on fit results. Moreover, we have shown that high-precision PIE-FCS measurements which are able to record all the 16 possible polarization-resolved fluorescence correlation curves, can be used to extract shape information about a macromolecule, within the limits of an ellipsoid-of-rotation model. We hope that the present Letter will help to make FCS more accessible for size and shape measurements of macromolecules.

Acknowledgments

The authors thank Ingo Gregor and Qui Van for fruitful discussions and valuable technical support. Financial support by the Deutsche Forschungsgemeinschaft (DFG, SFB 860, Project A6) is gratefully acknowledged.

References

[1] R. Kimmich, NMR-Tomography Diffusometry Relaxometry, Springer, 1997.
[2] J. Lipfert, S. Doniach, Annu. Rev. Biophys. Biomol. Struct. 36 (2007) 307.
[3] B.J. Berne, R. Pecora, Dynamic Light Scattering, John Wiley and Sons, 1976.
[4] J.R. Lakowicz, Principles of fluorescence spectroscopy, Springer, 2006.
[5] T.M. Jovin, M. Bartholdi, W.L. Vaz, R.H. Austin, Ann. NY Acad. Sci. 366 (1981) 176.
[6] F.N. Castellano, J.D. Dattelbaum, J.R. Lakowicz, Biochemistry 170 (1998) 165.
[7] F.L. González Flecha, V. Levi, Biochem. Mol. Biol. Ed. 31 (2003) 319.
[8] D. Magde, E. Elson, W. Webb, Phys. Rev. Lett. 29 (1972) 705.
[9] E.L. Elson, D. Magde, Biopolymers 13 (1974) 1.
[10] D. Magde, E.L. Elson, W.W. Webb, Biopolymers 13 (1974) 29.
[11] Y. Tian, M.M. Martinez, D. Pappas, Appl. Spectrosc. 65 (2011) 115.
[12] M. Ehrenberg, R. Rigler, Chem. Phys. 4 (1974) 390.
[13] S.R. Aragón, R. Pecora, Biopolymers 14 (1975) 119.
[14] E.W. Small, I. Isenberg, Biopolymers 16 (1977) 1907.
[15] P. Kask, P. Piksarv, U. Mets, M. Pooga, E. Lippmaa, Eur. Biophys. J. 14 (1987) 257.
[16] P. Kask, P. Piksarv, M. Pooga, U. Mets, E. Lippmaa, Biophys. J. 55 (1989) 213.
[17] S. Felekyan, R. Kühnemuth, V. Kudryavtsev, C. Sandhagen, W. Becker, C.A.M. Seidel, Rev. Sci. Instrum. (8) (2005) 08310 4.
[18] M. Dorfschmid, K. Müllen, A. Zumbusch, D. Wöll, Macromolecules 43 (2010) 6174.
[19] A. Loman, I. Gregor, C. Stutz, M. Mund, J. Enderlein, Photochem. Photobiol. Sci. 9 (2010) 627.
[20] K. Bahlmann, S.W. Hell, Appl. Phys. Lett. 77 (2000) 612.
[21] R. Feynman, Feynman's Lectures on Physics, Addison-Wesley, 1964.
[22] B.K. Müller, E. Zaychikov, C. Bräuchle, D.C. Lamb, Biophys. J. 89 (2005) 3508.
[23] F. Perrin, J. Phys. 7 (1934) 497.
[24] F. Perrin, J. Phys. 7 (1936) 1.
[25] S.H. Koenig, Biopolymers 14 (1975) 2421.
[26] E. Wolf, Math. Phys. Sci. 253 (1959) 349.
[27] B. Richards, E. Wolf, Proc. R. Soc. Lond. A Math. Phys. Sci. 253 (1959) 358.
[28] T. Ha, T.A. Laurence, D.S. Chemla, S. Weiss, J. Phys. Chem. B 103 (1999) 6839.
[29] J. Widengren, P. Schwille, Characterization of photoinduced isomerization and back-isomerization of the cyanine dye cy5 by fluorescence correlation spectroscopy, J. Phys. Chem. A 104 (2000) 6416.
[30] M. Wahl, I. Gregor, M. Patting, J. Enderlein. Opt. Express. 11 (2003) 3583–3591.

Christoph Pieper studied physics at the Georg-August-University from 2005 till 2010 and is now a grad student with the III. Institute of Physics (Biophysics). His main research topic is the fluorescence spectroscopic investigation of protein conformation, dynamics, and interaction.

Jörg Enderlein studied physics in Odessa (Ukraine) from 1981 until 1986, and obtained his Ph.D. in 1991 at the Humboldt-University in Berlin (Germany). After his postdoc time in the group of Richard A. Keller at Los Alamos National Laboratories in 1996/97, he started his own research group in Germany in the field of single molecule spectroscopy and imaging. Since 2008, he is full professor of physics at the Georg-August-University in Göttingen. His main fields of research are development of single-molecule spectroscopy and imaging methods for applications in biophysics, physical chemistry, and physics, as well as nano-optics.